# Solar Semidiurnal Tidal Wind Oscillations Above the CART Site

*C. D. Whiteman and X. Bian*
*Pacific Northwest National Laboratory*
*Richland, Washington*

Harmonic analysis of wintertime data from 915- and 404-MHz radar wind profilers at four sites in North America has identified coherent semidiurnal wind oscillations through the entire depth of the troposphere. These winds are readily apparent above the Cloud and Radiation Testbed (CART) site, as evidenced from analyses of data from the Haviland, Kansas, radar profiler. The characteristics of this wind system match the characteristics of solar semidiurnal atmospheric tides, as predicted by a simple dynamic model.

## Characteristics of the Observed Wind System

Our recent analyses of radar profiler wind data (Whiteman and Bian 1994, 1995a, 1995b) have identified semidiurnal wind oscillations in the troposphere that are consistent from site to site at four sites that are widely separated across the United States (Table 1 and Figure 1). For these analyses, the series of hourly wind data at each range gate and site were averaged vectorially for each hour of the day to produce a mean daily time-height cross section of vector winds. A harmonic analysis was then performed for the u- and v-components of the 24 vectors in the cross section for each range gate. The semidiurnal wind amplitudes and phases obtained from this analysis were consistent from site to site, despite widely differing geography and topography at the four sites. The coherent semidiurnal wind system first became apparent at altitudes above a 500- to 1000-m-deep frictional boundary layer. Tidal amplitudes were ~0.2 m/s there, but increased with elevation to attain 0.7 m/s at 5-7 km above mean sea level (MSL). The phases were consistent from site to site when calculated in local mean solar time and changed little with altitude at the four sites investigated, with the maximum northward (eastward) wind speeds attained at about 0100 (0400) apparent local solar time. The winds at a fixed height turned clockwise with time. This wind system behavior is shown in a hodograph representation in Figure 2. The characteristics of this semidiurnal circulation were compared with the results of a dynamic model used to simulate the characteristics of solar semidiurnal thermal atmospheric tides.

**Table 1**. Information on radar profiler sites and data sets.

| Site | ID | Latitude (°N) | Longitude (°W) | Elevation (m MSL) | Period of Record |
|---|---|---|---|---|---|
| **NOAA Wind Profiler Demonstration Network (404 MHz)** | | | | | |
| Hudson, Massachusetts | HUD | 42.41 | 71.48 | 93 | JFD 91 and JF 92 |
| Haviland, Kansas | HAV | 37.65 | 99.09 | 648 | JFD 91 and JF 92 |
| Platteville, Colorado | PLT | 40.18 | 104.72 | 1524 | JFD 91 and JF 92 |
| **Project MOHAVE (915 MHz)** | | | | | |
| Temple Bar, Arizona | TBR | 36.02 | 114.33 | 460 | 01/03/92-04/19/92 |

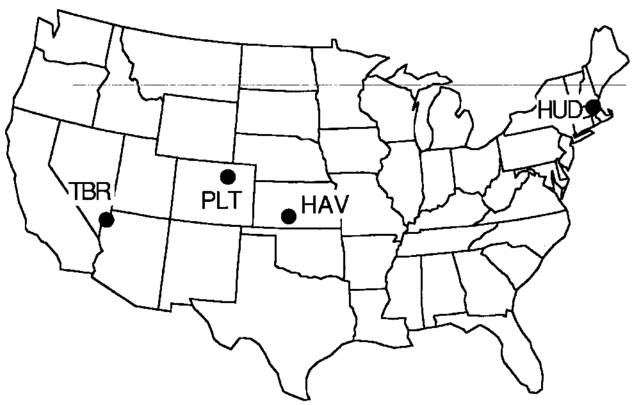


**Figure 1**. Radar profiler locations.

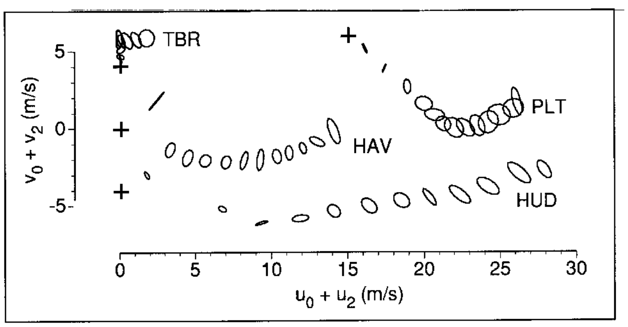


**Figure 2**. Hodograms of the sum of the mean daily (subscript 0) and mean hourly semidiurnal (subscript 2) wind components at the four sites. Twenty-four hourly points make up the elliptical wind figures for each range gate. Each of the hourly points can be thought of as defining the tip of a wind vector drawn from the coordinate origin, indicated for each site by a plus sign. This vector rotates clockwise twice per day around each of the hodograms. For use, the u- and v-component scales must be shifted to the origin for each of the sites. The first range gates are at 2024, 593, 637 and 1148 m MSL for HAV, HUD, PLT and TBR, respectively. Additional plotted range gates are at 500-m intervals for HAV, HUD and PLT, and at 406-m intervals for TBR, so that the highest plotted range gates are at 8024, 6093, 3885, and 6648 m MSL, respectively.

# Dynamical Model

Semidiurnal tidal wind characteristics are illustrated by solving the momentum equations for a frictionless atmosphere on a rotating earth:

$$\frac{\partial u}{\partial t} - 2\,\Omega\, v \sin\Phi = -\frac{1}{\rho R \cos\Phi}\frac{\partial p}{\partial \lambda}$$
$$\frac{\partial v}{\partial t} + 2\,\Omega\, u \sin\Phi = -\frac{1}{\rho R}\frac{\partial p}{\partial \Phi} \qquad (1)$$

where u and v denote, respectively, the eastward- and northward-directed semidiurnal wind components, $\Phi$ is latitude, $\lambda$ is longitude, $\Omega$ is the angular velocity of the earth, $\rho$ is air density, R is the earth's radius, and p is the pressure perturbation obtained from Haurwitz's (1956) global fit to observed semidiurnal surface pressure perturbation data

$$p = p_m \cos^3\Phi \sin[2(t' + \lambda) + \sigma] \qquad (2)$$

where $p_m$ is the amplitude of the semidiurnal pressure oscillation at the equator (1.16 hPa), t' is Universal Time (UT) reckoned in angle at the rate of 360° per mean solar day from lower transit (i.e., midnight), and $\sigma$ is the initial phase of the pressure perturbation (158°). The solutions to Equation 2 for the semidiurnal winds, from Chapman and Lindzen (1970), are

$$u = C_s\,(1 + 1.5 \sin^2\Phi) \sin(2t'' + 180^\circ + \sigma) \qquad (3)$$

$$v = 2.5\, C_s \sin\Phi \sin(2t'' + 90^\circ + \sigma) \qquad (4)$$

where $C_s$ = pm/$\rho$R = 0.2 m/s, and t" = t' + $\lambda$ is apparent local solar time. The maximum amplitudes of the u and v components at the mean latitude of the four sites is 0.3 m/s, and the maxima in the u and v components occur at 0344 (and 1544) and 0044 (and 1244) apparent local solar time, respectively. Thus, the modeled wind system characteristics match those of the observations. The modeled winds occur over the entire globe, turn clockwise with time at a given height, and have amplitudes and phases similar to those obtained from the radar profiler analyses.

# Conclusion

Since the winds observed with radar profilers have characteristics that match those of the solar thermal tides, as predicted by a simple dynamical model using observed surface semidiurnal pressure perturbations, we conclude that the observed winds are solar semidiurnal tides. This global tidal wind system is apparent in data collected near the CART site. Further investigations are under way to determine whether tidal convergence fields influence cloudiness and precipitation in the CART region.

# Acknowledgments

Research was supported by the U.S. Department of Energy (DOE) under Contract DE-AC06-76RLO 1830 at Pacific Northwest Laboratory as part of DOE's Atmospheric Studies in Complex Terrain and Atmospheric Radiation Measurement programs. Pacific Northwest National Laboratory is operated for the DOE by Battelle Memorial Institute.

# References

Chapman, S., and R. S. Lindzen. 1970. *Atmospheric Tides*. D. Reidel Publishing Co., Dordrecht, pp. 200.

Haurwitz, B. 1956. The geographical distribution of the solar semidiurnal pressure oscillation, *Meteor. Pap.*, **2**(5), New York University.

Whiteman, C. D., and X. Bian. 1994. Semidiurnal solar tides in the mountain atmosphere, 23 Internationale Tagung für Alpine Meteorologie, Lindau, Germany, *Annal. Meteor.*, **30**, 239-242. Deutscher Wetterdienst, Offenbach am Main, Germany.

Whiteman, C. D., and X. Bian. 1995a. Radar wind profiler observations of solar semidiurnal atmospheric tides, *Geophys. Res. Lett.*, **22**(8), 901-904.

Whiteman, C. D., and X. Bian. 1995b. Solar semidiurnal tidal winds in the troposphere, *Bull. Am. Met.*, accepted.